



CHORUS

This is the accepted manuscript made available via CHORUS. The article has been published as:

Efficiency of osmotic pipe flows

Louise Sejling Haaning, Kaare Hartvig Jensen, Claus Hélix-Nielsen, Kirstine Berg-Sørensen, and Tomas Bohr

Phys. Rev. E **87**, 053019 — Published 28 May 2013

DOI: [10.1103/PhysRevE.87.053019](https://doi.org/10.1103/PhysRevE.87.053019)

The Efficiency of Osmotic Pipe Flows

Louise Sejling Haaning,^{1,*} Kaare Hartvig Jensen,^{1,2,*} Claus Hélix-Nielsen,¹ Kirstine Berg-Sørensen,¹ and Tomas Bohr^{1,†}

¹*Department of Physics, Technical University of Denmark, Kongens Lyngby, DK-2800, Denmark*

²*Department of Organismic and Evolutionary Biology, Harvard University, Cambridge, MA 02138, USA*

We present experiments and theory for flows of sugar or salt solutions in cylindrical tubes with semi-permeable walls (hollow fiber membranes) immersed in water, quantifying the strength of the osmotic driving force in relation to the dimensionless parameters that specify the system. The pumping efficiency of these flows is limited by the presence of “unstirred” concentration boundary layers near the tube walls and our primary aim is to understand and quantify these layers and their effect on the flow. We measure the outlet flow rate Q_{out} while varying the inlet flow rate Q^* , concentration c^* , and tube length L , and map out the dependence of the flow rate gain $\gamma = Q_{\text{out}}/Q^* - 1$ on these parameters. A theoretical analysis based on (1) the known velocity field for slow flow in cylindrical porous tubes and (2) a parabolic concentration profile, allows us to compute analytically how the flow gain depends on the relative magnitude of radial diffusion and advection as well as the ratio of the osmotic velocity to pumping velocity, in very good agreement with experiments and with no adjustable parameters. Our analysis provides criteria that are useful for optimizing osmotic flow processes in e.g. water purification devices.

I. INTRODUCTION

Channel flows – liquid flows confined within a closed conduit with no free surfaces – are found in many natural and man-made systems. In animals [1] and plants [2] they serve as the building blocks of vascular systems, distributing energy to where it is needed and allowing distal parts of the organism to communicate. When constructed by humans, one of the major functions of channels is to transport liquids or gasses, e.g. water (irrigation and urban water systems) and energy (oil or natural gas) from sites of production to the consumer or industry. In some cases, the channels have solid walls which are impermeable to the liquid flowing inside. In other cases, the channels have semi-permeable membrane walls allowing solvent flux while rejecting solutes.

The effect of semi-permeable porous walls is especially important in the study of biological flows due to the presence of semi-permeable membranes and porous cell walls [2] and in industrial separation processes [3]. In these cases, the exchange of water across the membrane can be driven by either hydrostatic or osmotic pressure differences, thus modifying the bulk axial flow in the channel. A serious limitation to the performance of osmotic flows is that the entry of water into the tube lowers the solute concentration next to the membrane, as shown in Fig. 1. This negative feedback leads to a decrease in trans-membrane flow that can affect the efficiency of both natural and engineered systems, such as sugar transport in the phloem vasculature of plants and water purification in filtration devices. Osmotic flows are exceptionally complicated to analyse due to the intrinsic nonlinear nature of the flow which arises due to the coupling between

the velocity and concentration fields, see e.g. [4–9]. Only in a few cases have experiments been compared directly to theory, see e.g. [10–12].

In this article, we report experimental results of osmotic flows through a long, narrow cylindrical tube with porous walls. A simple continuum model predicts that the osmotic pumping efficiency is determined solely by two parameters: a Péclet number β (see Table I and II for parameter definitions) and the maximal osmotic velocity scaled by the inlet velocity Γ . These parameters characterize the unstirred layer effects and the relative importance of feed and osmotic flows. Moreover, we observe that the pumping efficiency scales in an unexpected way with the parameters in the problem and show that our model correctly accounts for this scaling.

II. EXPERIMENTS

We flow aqueous solutions of sucrose ($\text{C}_{12}\text{H}_{22}\text{O}_{11}$) and sodium chloride (NaCl) through an experimental setup that consists of a long, narrow cylindrical hollow fiber membrane tube immersed in a reservoir containing pure water. The hollow fiber membrane was kindly supplied by Dr. Wang Rong, Singapore Membrane Technology Center, Nanyang Technological University, Singapore. It was fabricated by interfacial polymerization of a polyethersulfone substrate as described in [13, 14] where the membrane used in this study is denoted the #B type. A picture and a schematic sketch of the setup is shown in Fig. 2. We control the inlet flow rate by connecting the membrane tube to a syringe pump (Chemyx Inc., Fusion 400) and at the outlet, the solution flows into a reservoir at atmospheric pressure. The inlet flow rate and the solute concentration is varied over an order of magnitude: the flow rate from $Q^* = 0.2 \text{ mm}^3/\text{s}$ to $Q^* = 1.7 \text{ mm}^3/\text{s}$ and the concentration from $c^* = 0.05 \text{ M}$ to 1 M for NaCl

* These authors contributed equally to this work

† tbohr@fysik.dtu.dk

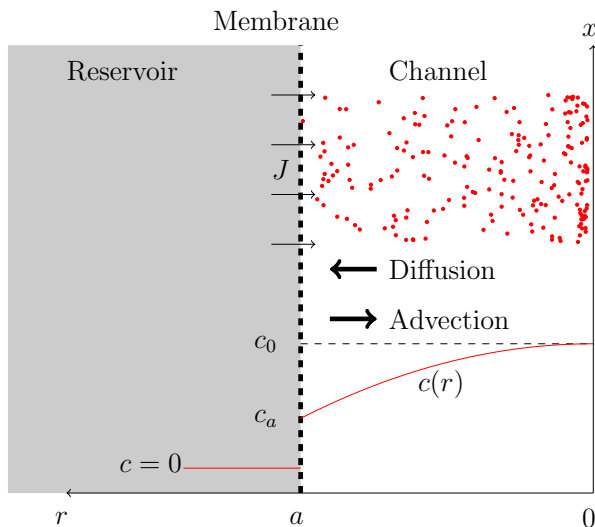


FIG. 1. (Color online) Sketch of the solute concentration $c(r)$ (solid red (gray) curve and density of dots) in a cylindrical tube of radius $r = a$ in contact with a reservoir containing pure solvent ($c = 0$). The semi-permeable membrane separating the two solutions is indicated by the thick dashed line. The concentration difference between the reservoir and channel drives an osmotic flow of solvent $J \propto c_a$ (thin arrows, see Eq. (2)) across the membrane. This dilutes the solution next to the membrane, and the concentration of solute in contact with the membrane $c_a = c(a)$ is therefore lower than the value $c_0 = c(0)$ at the center of the tube. The concentration profile $c(r)$ is set by the relative magnitude of diffusive and advective fluxes (thick arrows). At the membrane interface ($r = a$), there can be no net flux of solute molecules $J_s = -D\partial_c + Jc_a = 0$, which determines the relative magnitude of c_0 and c_a , see Eq. (13).

and from $c^* = 0.05$ M to 0.5 M for sucrose. The radius of the tube is held constant at $a = 0.5$ mm, while the length of the tube is varied from $L = 6.2$ cm to $L = 13.6$ cm. This approach allows us to measure the flow rate gain due to osmotic influx, defined as the ratio of outlet to inlet volumetric flow rates

$$\gamma = \frac{Q_{\text{out}}}{Q^*} - 1 = \frac{u_{\text{out}}}{u^*} - 1 \quad (1)$$

as a function of geometric and material properties of the problem. Here, Q_{out} and $u_{\text{out}} = Q_{\text{out}}/(\pi a^2)$ are the flow rate and average axial velocity at the outlet, respectively, and $u^* = Q^*/(\pi a^2)$ is the average inlet velocity.

We use a balance (Sartorius CP 423S) to measure mass flow at the outlet. Typical flow rate gains vary over two orders of magnitude from $\gamma = 0.1$ to $\gamma = 10$. A representative experimental graph is shown in Fig. 3(a). Here, the effect of varying inlet flow rate at fixed solute concentration is illustrated. At large inlet flow rates, the solute is advected quickly through the tube and the osmotic flow has little effect. At low flow rates, however, we ob-

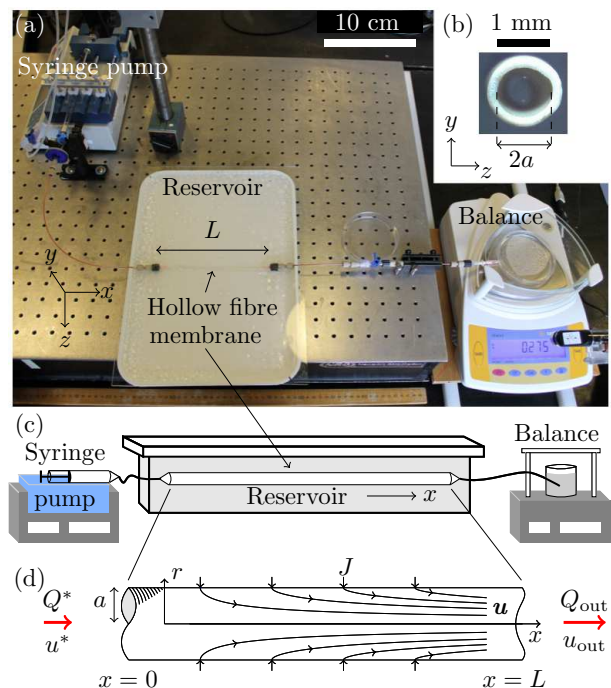


FIG. 2. Experimental setup. (a) Picture of the experimental setup. The syringe pump injects an aqueous solution of NaCl or sucrose into the hollow fiber membrane tube which is immersed in a reservoir containing pure water. The flow along the x -axis in the tube accelerates from the initial value Q^* due to osmotic exchange of water across the semi-permeable wall. We measure the resulting outlet rate Q_{out} using a balance. (b) Cross section view of the hollow fiber membrane tube. The inner diameter of the tube is $2a = 1$ mm and the wall thickness is $d \simeq 200 \mu\text{m}$. (c) Schematic of the experimental setup. (d) Sketch of the cylindrical flow geometry. The velocity field \mathbf{u} (streamline arrows, see Eqns. (5)-(6)) is determined by the average inlet flow velocity u^* and the trans-membrane flux J .

serve a strong gain. Similarly, Fig. (b) shows the effect of varying the solute concentration at fixed inlet flow rate. At low concentrations there is no net gain (i.e. $\gamma \ll 1$) since no osmotic flow occurs and we are simply observing the effect of the syringe pump. At $c^* = 1$ M, however, the gain is significant ($\gamma \simeq 1$) and the axial flow in the membrane tube is strongly influenced by the osmotic pumping. To quantify the pumping process, we measure the gain as a function of inlet flow rate Q^* , and inlet solute concentration c^* for two different solutes which yields a total of 216 data points, shown in Fig. 3(c-d).

III. THEORY OF OSMOTIC PIPE FLOWS

As previously described, we propose that the flow of water across the membrane wall is driven by osmotic pressure differences with a modification due to the presence of concentration boundary layers. Aldis was the first

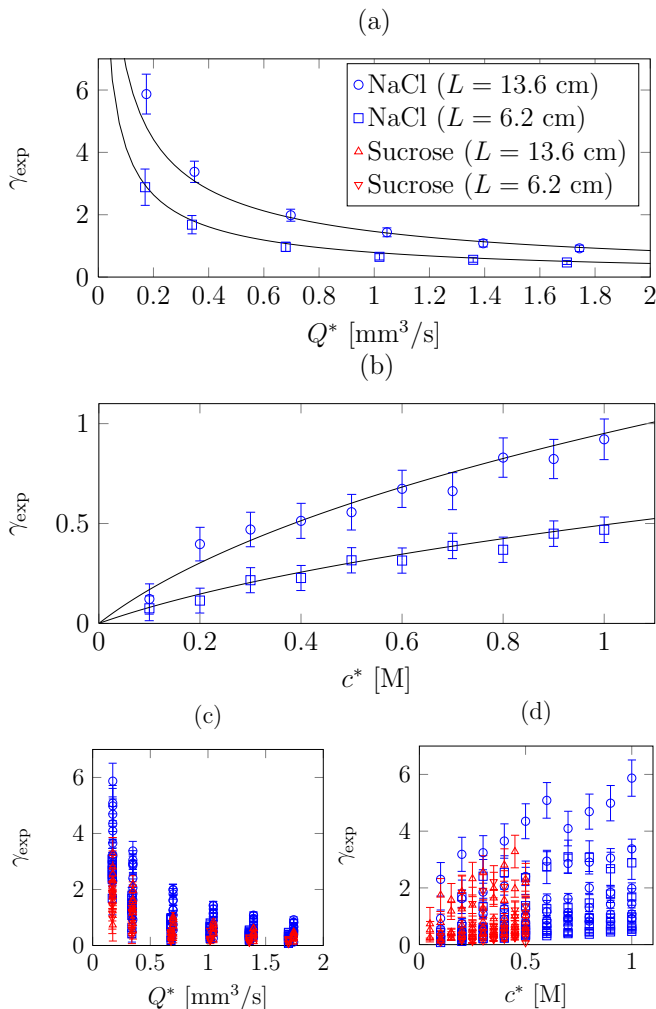


FIG. 3. (Color online) Experimental data, recorded with NaCl (a-d) and sucrose (c-d) as the solute, as indicated in the legend of (a). (a) Flow rate gain $\gamma = Q_{\text{out}}/Q^* - 1$ plotted as a function of inlet flow rate Q^* for constant inlet NaCl concentration $c^* = 1.0$ M. (b) Flow rate gain γ plotted as a function of inlet NaCl concentration c^* for constant inlet flow rate $Q^* = 1.7$ mm³/s. In (a) and (b), solid lines show theoretical predictions from Eq. (24) with no free parameters. In (c) and (d), experimental data from all 216 experiments using sucrose and NaCl are shown. Error bars in (a)-(d) indicate the errors obtained in the least squares fits to the slopes of the linear (time, mass)-data curves measured using the balance shown in Fig. 2.

TABLE I. Non-dimensional parameters.

aspect ratio	α	$= aL^{-1}$	0.004 – 0.008
flow rate gain	γ	$= Q_{\text{out}}(Q^*)^{-1} - 1$	0.1 – 10
max flow rate gain	Γ	$= 2L_p RTc^* L(u^*a)^{-1}$	0.08 – 20
concentration variation	ϕ	$= (c_0 - c_a)/c_a$	0.04 – 1.1
Péclet number			
- axial	Pe_x	$= u^*LD^{-1}$	$10^3 - 10^5$
- radial	Pe_r	$= L_p RTc^* aD^{-1}$	0.3 – 3.9
- mixed	Pe	$= u^*aD^{-1}$	68 – 2100
- boundary layer	β	$= u^*a^2(6DL)^{-1}$	0.04 – 2.8
Reynolds number	Re	$= \rho u^* a\eta^{-1}$	0.1 – 1

TABLE II. Material parameters at $T = 20^\circ\text{C}$. Values for D , R , and η were obtained from [15]

tube radius	a	500 μm
concentration at inlet	c^*	0.05 – 1 M
thickness of membrane tube wall	d	200 μm
diffusion coefficient	D	$5.2 \times 10^{-10} \text{ m}^2 \text{ s}^{-1}$ (S)
		$1.6 \times 10^{-9} \text{ m}^2 \text{ s}^{-1}$ (NaCl)
length of membrane tube	L	6.2 cm, 13.6 cm
permeability of membrane	L_p	$3.3 \times 10^{-12} \text{ m s}^{-1} \text{ Pa}^{-1}$
flow rate at inlet	Q^*	0.2 – 2 mm ³ s ⁻¹
gas constant	R	8.314 J K ⁻¹ mol ⁻¹
absolute temperature	T	293 K
velocity at inlet	u^*	60 – 600 $\mu\text{m s}^{-1}$
viscosity	η	1 – 5 mPa s

to considered the effect of unstirred layers on osmotic flow in a cylindrical tube [11]. He found analytical solutions for the concentration and velocity fields in the limit of strong radial diffusion (boundary layer effects negligible) and for short distances using a series expansion. Our experiments, however, satisfy neither of these criteria and we proceed to analyse the problem in the general case.

We begin by writing the water flux J across the semi-permeable tube wall as

$$J = L_p(RT\Delta c - \Delta p) \quad (2)$$

where L_p is the permeability of the membrane, R is the gas constant, T is the absolute temperature, Δc is the difference in solute concentration, and Δp is the difference in hydrostatic pressure between the inside and the outside of the tube. See Appendix A for details on how L_p was measured. For clarity we use the van't Hoff value $RT\Delta c$ for the osmotic pressure in Eq. (2), which is valid only for dilute (ideal) solutions. At the concentrations relevant to our experiments ($c < 1$ M for NaCl and $c < 0.5$ M for sucrose), the error in the osmotic pressure introduced by using the van't Hoff value is $\sim 10\%$ [17]. The liquid outside the tube is pure water ($c = 0$), so the concentration difference $\Delta c = c_a$ where c_a is the concentration at the inner surface of the tube ($r = a$, see Fig. 1 and 2). Viscous friction which is responsible for the term Δp in Eq. (2), typically creates pressures of the order $\Delta p \simeq 8\eta u^*L/a^2 \simeq 1$ Pa where $\eta \simeq 1 - 5$ mPa s is the viscosity of the solution. These pressures are much smaller than the osmotic pressure differences $RT\Delta c \simeq 10^5$ Pa and it is therefore safe to disregard the Δp term in Eq. (2) and write instead $J = L_p RTc_a$.

The radial flux J , of water in or out of the tube is naturally related to the mean axial flow velocity u along the x -axis via volume conservation: $\partial_x u = 2J/a$. We therefore have the following equation for the average axial velocity

$$\partial_x u = 2 \frac{L_p}{a} RTc_a \quad (3)$$

The concentration c is governed by the advection-diffusion equation

$$\partial_t c + \mathbf{u} \cdot \nabla c = D \nabla^2 c \quad (4)$$

where D is the diffusion coefficient of the solute in water (see Table II). The 3-D flow field $\mathbf{u} = (u_x, u_r, u_\theta)$ will generally be complicated, but since the channel Reynolds number $Re = \rho u^* a / \eta \simeq 0.1$ and aspect ratio $\alpha = a/L \simeq 0.005$ are both reasonably small we expect the flow to be rotationally symmetric, laminar and to have a Poiseuille axial flow profile. As shown by e.g. Aldis [10], the velocity field $\mathbf{u} = (u_x, u_r)$ in cylindrical coordinates is then given by

$$u_x = 2 \frac{(a^2 - r^2)}{a^2} u(x) \quad (5)$$

$$u_r = \frac{r(r^2 - 2a^2)}{a^3} J(x) \quad (6)$$

The hollow fiber membrane used in the experiments is able to retain ion-sized solutes. Moreover, axial diffusion plays very little role since the axial Péclet number $Pe_x = u^* L / D \simeq 10^4$ is large. Therefore, assuming steady state and taking the radial average of Eq. (4) implies that the axial solute flux is a conserved quantity, i.e.,

$$\langle cu \rangle = \text{const} = c^* u^* \quad (7)$$

where $\langle cu \rangle = 2/a^2 \int_0^a u_x(r) c(r) r dr$. Of the concentration field $c(r, x)$ we know that the radial solute flux

$$J_c = -D \partial_r c + u_r c \quad (8)$$

must vanish at $r = 0$ and $r = a$ in order to satisfy the no-flux boundary condition at the channel center line and at the membrane wall. Eq. (8) leads to

$$\partial_r c = 0 \quad \text{at} \quad r = 0 \quad (9)$$

$$-D \partial_r c - L_p R T c^2 = 0 \quad \text{at} \quad r = a \quad (10)$$

When radial diffusion dominates, the difference in concentration across the tube will be small, specifically where the local Péclet number $J(x) a / D = L_p R T c_a(x) a / D$ is small. In this limit, it is reasonable to assume that the concentration gradient at the membrane is of the order $(c_a - c_0) / a$, where $c_0(x)$ is the concentration at $r = 0$. To solve the averaged advection-diffusion equation (7), together with the boundary conditions in Eq. (9) and (10), we approximate the concentration profile by a parabolic function

$$c(r) = c_0(x) + (c_a(x) - c_0(x)) \frac{r^2}{a^2} \quad (11)$$

Since the advection-diffusion equation can be written entirely in terms of $\rho = r^2$ [18], we can safely neglect odd terms in r in the profile. The functional form of Eq. (11) is sketched in Fig. 1. In this approximation, the no-flux boundary condition at $r = a$ (Eq. (10)) is

$$-\frac{2D(c_a - c_0)}{a} - L_p R T c_a^2 = 0 \quad (12)$$

which sets a relation between the concentration at the channel center c_0 and wall c_a

$$c_0 = c_a + \frac{L_p R T a}{2D} c_a^2 = c_a + \frac{P e_r}{2} \frac{c_a^2}{c^*} \quad (13)$$

where $P e_r = L_p R T c^* a / D$ is the radial Péclet number.

From the conservation of solute flux (Eq. (7)), we now have from Eqns. (5) and (11)

$$\left(c_a + \frac{P e_r}{3} \frac{c_a^2}{c^*} \right) u = u^* c^* \quad (14)$$

To eliminate c_a from Eq. (14) we use Eq. (3) which leads to

$$\left(\frac{a}{2L_p R T} \partial_x u + \frac{P e_r}{3c^*} \left(\frac{a}{2L_p R T} \partial_x u \right)^2 \right) u = c^* u^* \quad (15)$$

Introducing the variables $X = x/L$ and $U = u/u^*$, Eq. (15) can be written in non-dimensional form

$$\left(\partial_X U + \beta (\partial_X U)^2 \right) U = \Gamma \quad (16)$$

where

$$\Gamma = 2 \frac{L}{a} \frac{L_p R T c^*}{u^*} \quad (17)$$

is the ratio of the largest obtainable purely osmotic flow velocity $2\pi a L L_p R T c^* / (\pi a^2)$ and the inlet velocity u^* . The parameter

$$\beta = \frac{1}{6} \frac{a}{L} \frac{u^* a}{D} = \frac{1}{3} \frac{P e_r}{\Gamma} = \frac{1}{6} \alpha P e \quad (18)$$

is proportional to the ratio of the radial Péclet number $P e_r$ and the maximum flow gain Γ , or, to the product of the aspect ratio α and the mixed Péclet number $P e = u^* a / D$.

In the non-dimensional formulation, the flow rate gain is given by $\gamma = U(1) - 1$, and Γ thus provides an upper limit to the pumping efficiency, since we must have $\gamma \leq \Gamma$. An implicit solution of Eq. (16) can be obtained by the Legendre transformation $X = \partial_t y$, $U = t \partial_t y - y$, and $\partial_X U = t$. With this change of coordinates, Eq. (16) leads to a linear equation in $y(t)$

$$(t^2 + \beta t^3) \partial_t y - (t + \beta t^2) y = \Gamma \quad (19)$$

which has the solution

$$y(t) = \Gamma \left[-\frac{1}{2t} + \beta + t \beta^2 \log \left(\frac{t}{1 + \beta t} \right) \right] + tC \quad (20)$$

where the constant C allows us to fulfill the boundary condition $U(X(t) = 0) = 1$ (in dimensional coordinates: $u(0) = u^*$). The non-dimensional velocity $U(X(t))$ and axial coordinate $X(t)$ can be written in terms of t as

$$X = \Gamma \left[\frac{1}{2t^2} + \frac{\beta^2}{1 + \beta t} + \beta^2 \log \left(\frac{t}{1 + \beta t} \right) \right] + C \quad (21)$$

$$U = \frac{\Gamma}{t + \beta t^2} \quad (22)$$

To determine C , we note that $U = 1$ when $t = t_0 = (-1 + \sqrt{1 + 4\Gamma\beta}) / (2\beta)$. By inserting t_0 in Eq. (21) with $X = 0$, we find that

$$C = -\Gamma \left[\frac{1}{2t_0^2} + \frac{\beta^2}{1 + \beta t_0} + \beta^2 \log \left(\frac{t_0}{1 + \beta t_0} \right) \right] \quad (23)$$

The flow rate gain γ can finally be determined from

$$\gamma(\beta, \Gamma) = U(1) - 1 = \frac{\Gamma}{t_1 + \beta t_1^2} - 1 \quad (24)$$

where t_1 is found from Eq. (21) by solving $X(t_1) = 1$.

The flow rate gain γ predicted by Eq. (24) is plotted as a function of β and Γ in Fig. 4(a). In Fig. 4(b), it is compared to measured values of γ from 216 experiments. Over two orders of magnitude of variation in γ , we find excellent agreement between the experimental data and the prediction of Eq. (24) with no free parameters.

When deriving Eq. (24), we approximated the concentration by the parabolic profile given in Eq. (11) under the assumption that the radial concentration distribution was close to uniform. To check this condition we consider the magnitude of $\phi = (c_0 - c_a)/c_a$. If $\phi = 0$, the concentration profile is completely flat while if $\phi = 1$ the concentration varies by a factor of 2 across the tube. Using Eqns. (13), (3), and (16), ϕ can be written as

$$\phi = \frac{c_0 - c_a}{c_a} = \frac{3}{4} \left(\sqrt{1 + \frac{4 Pe_r}{3 U}} - 1 \right) \quad (25)$$

In a given experiment, the non-dimensional velocity $U = u/u^*$ varies between 1 and $\gamma + 1$ along the tube (see Eq. (1)). This observation leads to the following inequality for ϕ

$$\frac{3}{4} \left(\sqrt{1 + \frac{4 Pe_r}{3(1+\gamma)}} - 1 \right) < \phi < \frac{3}{4} \left(\sqrt{1 + \frac{4 Pe_r}{3}} - 1 \right) \quad (26)$$

Using measured values of γ and calculated values of Pe_r , we find that ϕ varies between 0.04 and 1.1, indicating that there is at most a 50% variation in concentration across the tube, in rough accord with the slowly varying concentration approximation.

A. Limiting cases

In the majority of our experiments, both β and Γ are of moderate magnitude (see Fig. 4(a) and Table II). It is therefore likely that the boundary layer contributes significantly to the flow and that the full solution of Eq. (16) is needed to rationalize the experimental data. It is, however, of general interest to consider limiting cases of Eq. (16) and we therefore consider solutions for $\beta \ll 1$ and $\beta \gg 1$ for arbitrary values of Γ below. Taking $\Gamma \ll 1$ leads to $u(x) = u^*$ (i.e. $\gamma = 0$), and is therefore of limited interest since we generally look for conditions that optimise the osmotic flow and thus maximize γ .

1. Weak unstirred concentration boundary layer effects

Consider the situation where radial diffusion is strong compared to both radial and axial advection. In this case

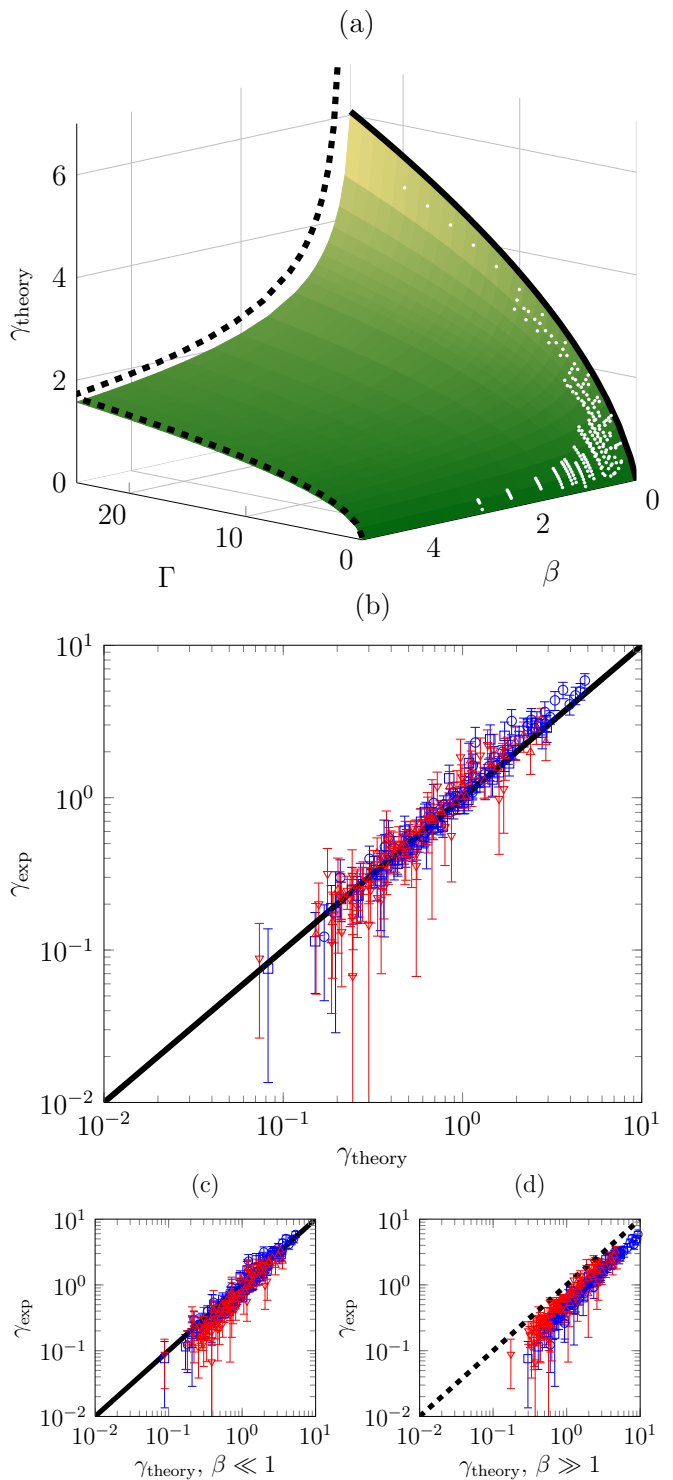


FIG. 4. (Color online) Comparison between experimental and theoretical values of the flow rate gain γ . (a) Green (gray) surface shows theoretical predicted values of γ (Eq. (24)) plotted as a function of β and Γ . The solid black line indicates the approximate analytical solutions for $\beta \ll 1$ (Eq. (28)). The black dashed lines indicate the approximate analytical solutions for $\beta \gg 1$ (Eq. (30)). White dots indicate the location in the (β, Γ) -plane of experimental data points. (b) Measured values of γ plotted as a function of the predicted values using Eq. (24). (c) Measured values of γ plotted as a function of the predicted values using Eq. (28). (d) Measured values of γ plotted as a function of the predicted values using Eq. (30). (b)-(d) uses the same legend as Fig. 3(a).

the radial and mixed Péclet numbers $Pe_r = L_p RT c^* a / D$ and $Pe = u^* a / D$ are small. This implies (i) that the concentration is nearly uniform ($\phi \sim Pe_r \ll 1$, see Eq. (25)), and (ii) that the parameter $\beta \sim \alpha Pe \ll 1$ (see Eq. (18)) when the aspect ratio $\alpha = a/L$ is small, as is generally the case in our experiments. In this limit, the solution of Eq. (16) is

$$U(X) = (1 + 2\Gamma X)^{1/2} \quad (27)$$

which has previously been found by e.g. Aldis [11] and Thompson and Holbrook [19]. In this limit, the flow rate gain γ can be expressed as

$$\gamma + 1 = (1 + 2\Gamma)^{1/2} = \left(1 + \frac{4L_p RT c^* L}{u^* a}\right)^{1/2} \quad (28)$$

shown in Fig. 4(a) as a solid line. Eq. (28) provides a useful approximation to γ for small values of β .

2. Strong unstirred concentration boundary layer effects

When radial diffusion becomes comparable or weaker than radial and axial advection, both the radial and the mixed Péclet numbers $Pe_r = L_p RT c^* a / D$ and $Pe = u^* a / D$ can become greater than 1. In this limit the concentration profile in the tube is no longer uniform ($\phi \geq 1$, see Eq. (25)) and the magnitude of the parameter β can exceed unity. Keeping in mind that that our experiments have only confirmed the validity of Eq. (16) for $\beta \leq 2.8$, we proceed to consider the case $\beta \gg 1$. In this limit, the solution of Eq. (16) is

$$U(X) = \left[\frac{3}{2} \left(\frac{\Gamma}{\beta} \right)^{1/2} X + 1 \right]^{2/3} \quad (29)$$

The flow rate gain γ can be expressed as

$$\gamma + 1 = \left[\frac{3}{2} \left(\frac{\Gamma}{\beta} \right)^{1/2} + 1 \right]^{2/3} \quad (30)$$

$$= \left[\frac{3}{2} \left(\frac{12L_p RT c^* L^2 D}{a^3 (u^*)^2} \right)^{1/2} + 1 \right]^{2/3} \quad (31)$$

shown in Fig. 4(a) as dashed lines. Eq. (30) provides a simple approximation to Eq. (24) for large values of β/Γ , where the flow rate gain scales as $\gamma \propto (\Gamma/\beta)^{1/2}$. For $\beta \geq 1$ and $\Gamma \geq 1$ the error in Eq. (30) is typically less than 10% when compared to Eq. (24).

The flow rate gains predicted by Eqns. (28) and (30) are compared to the experimentally obtained values in Fig. 4(c)-(d), and the relative error $(\gamma_{\text{exp}} - \gamma_{\text{theory}})/\gamma_{\text{exp}}$ is plotted as a function of β in Fig. 5. While both Eq. (28) and (30) show reasonable agreement between theory and experiment, the deviation between theory and experiment clearly depends on the value of β . Fig. 5 thus illustrates that the parameter β plays an important qualitative role in determining the scaling of the flow rate gain γ with the parameters of the problem.

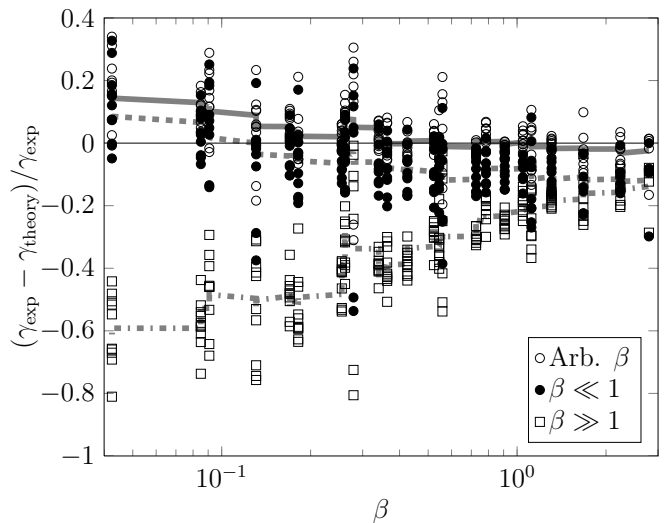


FIG. 5. Comparison between experimental and theoretical values of the flow rate gain γ . Relative error $(\gamma_{\text{exp}} - \gamma_{\text{theory}})/\gamma_{\text{exp}}$ plotted as a function of the Péclet number β for the full model (Eq. (24), open circles and solid line), the limit $\beta \ll 1$ (Eq. (28), dots and dashed line) and the limit $\beta \gg 1$ (Eq. (30), squares and dashed-dotted line). Lines show smoothed data curves as a guide to the eye (averaged over 20 neighboring data points).

IV. CONCLUSION AND DISCUSSION

In this paper, we have studied the effect of concentration boundary layers on osmotic flows in cylindrical tubes with porous walls. By varying the inlet flow rate Q^* , inlet solute concentration c^* , and tube length L , we have experimentally documented the dependence of the flow rate gain γ (Eq. (1)) on these parameters.

To explain our experimental observations, we have developed a simple model. The model quantifies the change in axial flow velocity due to osmotic exchange of water across the tube wall, and gives a first approximation to the effect of concentration boundary layers (Eq. (24)). We have compared theory and experiment with good results, as shown in Fig. 4(b).

Our theoretical predictions give interesting indications of how to develop and optimize devices that utilize osmotic pumps, such as membrane modules for forward osmosis applications based on hollow fibers [20, 21]. To obtain the greatest osmotic effect, it is clearly desirable to maximize Γ and minimize β , see Fig. 4(a). This can be done in a number of ways, e.g. by using a long membrane tube ($\Gamma \propto L$, $\beta \propto L^{-1}$), or by injecting fluid slowly ($\beta \propto u^*$, $\Gamma \propto (u^*)^{-1}$). The greatest potential for improvement, however, is in making the tube radius a as small as possible, since $\beta \propto a^2$ and $\Gamma \propto a^{-1}$. This increase in γ , however, will only continue as long as the back pressure due to viscous resistance $\Delta p \simeq 8\eta L u^* / a^2$ remains small compared to the osmotic pressure $RT c^* \simeq 10^5$ Pa, c.f Eq. (2). For water ($\eta = 1$

mPa s) flowing at $u^* = 1$ mm/s in a $L = 1$ m tube, the two pressures are of equal magnitude when $a \simeq 100 \mu\text{m}$. This indicates that using sub- $100 \mu\text{m}$ tubes in filtration devices is undesirable, although a more thorough analysis is needed to determine the optimum tube dimensions in the presence of viscous effects, and more generally non-linear concentration effects such as deviations from the van't Hoff relation.

V. ACKNOWLEDGEMENTS

The authors wish to thank Dr. Wang Rong, Singapore Membrane Technology Center, Nanyang Technolog-

ical University, Singapore for supplying the hollow fiber membrane and for helpful discussions. This work was supported by the Materials Research Science and Engineering Center (MRSEC, grant number DMR-0820484) at Harvard University and the Danish Council for Independent Research | Natural Sciences.

-
- [1] M. LaBarbera, *Science* **249**, 992 (1990).
- [2] N. M. Holbrook and M. Zwieniecki, eds., *Vascular transport in plants* (Academic Press, 2005).
- [3] C. H. Nielsen, *Analytical and bioanalytical chemistry* **395**, 697 (2009).
- [4] J. Dainty, *Protoplasma* **57**, 220 (1963).
- [5] T. J. Pedley and J. Fischbarg, *J. Theor. Biol.* **78**, 427 (1978).
- [6] T. J. Pedley, *Journal of Fluid Mechanics* **101**, 843 (1980).
- [7] T. J. Pedley, *Journal of Fluid Mechanics* **107**, 281 (1981).
- [8] T. J. Pedley, *Quarterly Reviews of Biophysics* **16**, 115 (1983).
- [9] K. H. Jensen, T. Bohr, and H. Bruus, *Journal of Fluid Mechanics* **662**, 197 (2010).
- [10] G. K. Aldis, *Bulletin of Mathematical Biology* **50**, 531 (1988).
- [11] G. K. Aldis, *Bulletin of Mathematical Biology* **50**, 547 (1988).
- [12] P. Pohl, S. M. Saparov, and Y. N. Antonenko, *Biophysical Journal* **75**, 1403 (1998).
- [13] R. Wang, L. Shi, C. Y. Tang, S. Chou, C. Qiu, and A. G. Fane, *Journal of Membrane Science* **355**, 158 (2010).
- [14] S. Chou, L. Shi, R. Wang, C. Y. Tang, C. Qiu, and A. G. Fane, *Desalination* **261**, 365 (2010).
- [15] W. M. Haynes, ed., *CRC Handbook of Chemistry and Physics*, 93rd ed. (CRC Press, Boca Raton, FL, 2012).
- [16] E. J. Stadelmann, *Methods in Cell Physiology vol. II*, edited by D. M. Prescott (Academic Press, New York, NY, 1966) pp. 144–216.
- [17] T. Y. Cath, A. E. Childress, and M. Elimelech, *Journal of Membrane Science* **281**, 70 (2006).
- [18] It can be shown that the advection-diffusion equation $\mathbf{u} \cdot \nabla c = D\nabla^2 c$ can be written in terms of $\rho = r^2$ and that the power series expansion of $c(r, x)$ contains only even powers of ρ .
- [19] M. V. Thompson and N. M. Holbrook, *Plant, Cell and Environment* **26**, 1561 (2003).
- [20] C. Tang, Y. Zhao, R. Wang, C. Hélix-Nielsen, and A. Fane, *Desalination* (2012), 10.1016/j.desal.2012.07.007.
- [21] Y. Zhao, C. Qiu, X. Li, A. Vararattanavech, W. Shen, J. Torres, C. Hélix-Nielsen, R. Wang, X. Hu, A. G. Fane, and C. Y. Tang, *Journal of Membrane Science* **423-424**, 422 (2012).
- [22] L. Shi, S. Chou, R. Wang, W. Fang, C. Tang, and a.G. Fane, *Journal of Membrane Science* **382**, 116 (2011).

Appendix A: Membrane permeability

The membrane permeability L_p was determined by applying a known hydrostatic pressure differential Δp across a membrane section of area A . By measuring the resulting flow rate Q , the permeability $L_p = Q/(A\Delta p)$ of the hollow fiber membrane was determined to be $L_p = (3.28 \pm 0.02) \times 10^{-12}$ m/s/Pa, consistent with values obtained from measurements on this type of membrane material [22].